

Hexagonal Boron Nitride: The Thinnest Insulating Barrier to Microbial Corrosion

Govinda Chilkkoor,[†] Sushma Priyanka Karanam,[‡] Shane Star,[†] Namita Shrestha,[†] Rajesh K. Sani,[§] Venkata K.K. Upadhyayula,^{||} Debjit Ghoshal,[⊥] Nikhil A. Koratkar,^{#,¶,○} M. Meyyappan,[△] and Venkataramana Gadhamshetty*,^{†,△,○}

[†]Civil and Environmental Engineering, [‡]Materials and Metallurgical Engineering, [§]Chemical and Biological Engineering, and [△]Surface Engineering Research Center, South Dakota School of Mines and Technology, 501 E. Saint Joseph Boulevard, Rapid City, South Dakota 57701, United States

^{||}Green Technologies and Environmental Economics Platform, Chemistry Department, Umeå University, Umeå, Sweden, 90187

[⊥]Department of Chemical and Biological Engineering, [#]Department of Mechanical, Aerospace and Nuclear Engineering, and

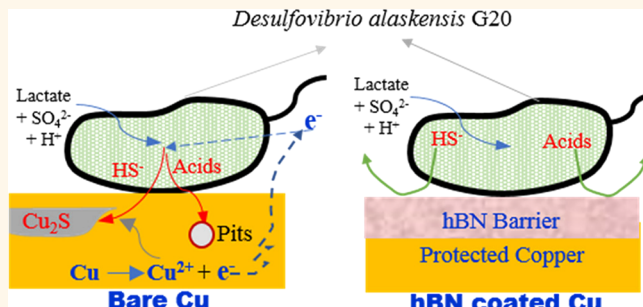
[¶]Department of Materials Science and Engineering, Rensselaer Polytechnic Institute, 110 Eighth Street, Troy, New York 12180-3590, United States

[○]Center for Nanotechnology, NASA Ames Research Center, Moffett Field, Mountain View, California 94035, United States

S Supporting Information

ABSTRACT: We report the use of a single layer of two-dimensional hexagonal boron nitride (SL-hBN) as the thinnest insulating barrier to microbial corrosion induced by the sulfate-reducing bacteria *Desulfovibrio alaskensis* G20. We used electrochemical methods to assess the corrosion resistance of SL-hBN on copper against the effects of both the planktonic and sessile forms of the sulfate-reducing bacteria. Cyclic voltammetry results show that SL-hBN-Cu is effective in suppressing corrosion effects of the planktonic cells at potentials as high as 0.2 V (vs Ag/AgCl). The peak anodic current for the SL-hBN coatings is ~36 times lower than that of bare Cu. Linear polarization resistance tests confirm that the SL-hBN coatings serve as a barrier against corrosive effects of the G20 biofilm when compared to bare Cu. The SL-hBN serves as an impermeable barrier to aggressive metabolites and offers ~91% corrosion inhibition efficiency, which is comparable to much thicker commercial coatings such as polyaniline. In addition to impermeability, the insulating nature of SL-hBN suppresses galvanic effects and improves its ability to combat microbial corrosion.

KEYWORDS: 2D coatings, hexagonal boron nitride, microbial corrosion, sulfate-reducing bacteria



Microbially induced corrosion (MIC) results in an unanticipated attack on metals in seemingly benign environments and threatens a range of multi-billion-dollar industries including aviation, surface transportation, and water infrastructure.¹ MIC accounts for 20–40% of the annual corrosion costs including direct and indirect impacts, which have been estimated to reach as high as \$1 trillion.² MIC poses a significant financial burden in the U.S. alone in the form of total direct costs (\$30–\$50 billion/year),³ biocide requirements (\$1.2 billion/year),⁴ and direct costs in oil and gas industries (\$2 billion/year).⁵ The U.S. annually spends nearly \$6 billion to combat MIC effects of sulfate-reducing bacteria (SRB) alone.⁶ The SRBs secrete exopolymers on metal surfaces and form a biofilm to induce uniform corrosion or localized pitting attack using one or more of the following mechanisms:⁷ (i) disruption of passivating metal-oxide films, (ii) altering

redox conditions at the metal–solution interface, (iii) regeneration of the electron acceptors, (iv) production of aggressive metabolites (e.g., sulfides), and (v) depolarizing the cathodic reactions.

Major corrosion mitigation practices including protective coatings and impressed current cathodic protection tend to fail under MIC conditions. For example, commercially available polymer coatings (e.g., epoxy liners) are prone to biodegradation, and they exhibit poor adhesion toward metals under aqueous conditions.^{8–11} The thickness of commercial coatings (~50–1000 μm) can also disrupt the functionality (e.g.,

Received: August 31, 2017

Accepted: February 12, 2018

Published: February 12, 2018

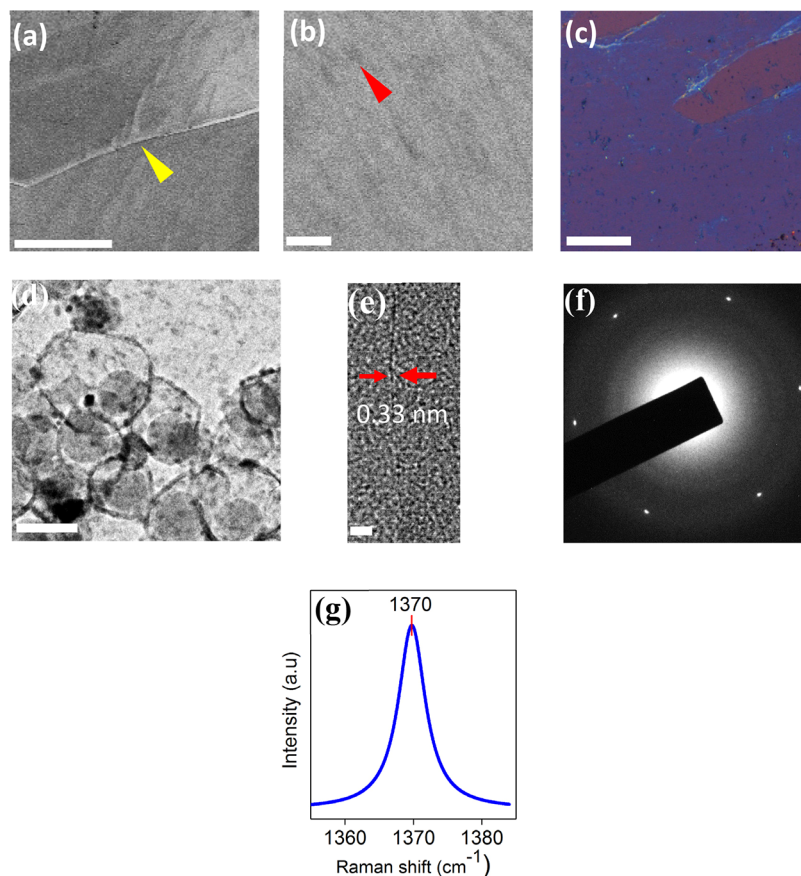


Figure 1. SEM, optical image, TEM and Raman characterization of as grown single layer hBN (SL-hBN). (a) The line in lower magnification SEM image (indicated with yellow arrow) represent a Cu grain boundary and the dark patches are the Cu domains. Scale bar: 100 μm . (b) The smaller scale faint grey zones (indicated in red arrow) in higher magnification SEM image represent few layered hBN films. Scale bar: 2 μm . (c) Optical image of SL-hBN (light indigo) transferred onto a SiO_2/Si substrate (background color). Scale bar: 50 μm . (d) TEM image showing sheets of SL-hBN. Scale bar: 50 nm. (e) TEM image of folded edge showing a single parallel line confirming the presence of SL-hBN. Scale bar: 2 nm. (f) Selected area electron diffraction pattern shows the crystalline and hexagonal nature of SL-hBN. (g) Typical Raman spectra for SL-hBN.

electrical conductivity, porosity, dimensional tolerances) of the underlying metals. Furthermore, SRB can accelerate the corrosion cells present under cathodic protection systems through cathodic depolarization by consuming hydrogen.

Recent studies have demonstrated the corrosion resistance of graphene-based materials^{1,12–15} under both abiotic and MIC conditions. The graphene coatings exhibit excellent chemical inertness, ductility, hydrophobicity, impermeability, and strength. Screening-level life cycle analysis has demonstrated environmental benefits of graphene coatings compared to zinc coatings, under both aggressive atmospheric corrosion¹⁵ and MIC conditions.^{16,17} However, the nanoscale defects in graphene coatings serve as cathodic sites for capturing and reducing terminal electron acceptors and simultaneously aggravating galvanic corrosion of the underlying metals.¹⁸ Unlike graphene, the 2D hexagonal boron nitrided (hBN) can be obtained as an insulating coating to suppress the galvanic effects. The 2D hBN materials have been reported to yield high-performance coatings endowed with exceptional properties related to adhesion, barrier, impermeability, and stability.^{18–21} The hBN-coated metals (e.g., Cu and steel) show oxidation resistance against corrosive effects of high temperatures (1100 °C)²² and harsh chemicals.^{18,23,24} 2D hBN-coated Cu has been shown to be an excellent barrier against Gram-negative *Escherichia coli*.¹⁹

In this paper, we explore the use of a single-layered hBN coating as a thinnest insulating barrier to protect metals against MIC effects of aggressive sulfate-reducing conditions. We use *Desulfovibrio alaskensis* G20 as the model for the SRB and Cu as a technologically relevant metal. This study provides insight into the performance of 2D hBN coating against the MIC effects of the G20 strain in the planktonic and sessile forms. Here, we assess and quantify the long-term performance of 2D hBN coating on a temporal scale that reflects Cu/biofilm dynamics in corrosion cells that are continuously operated under a fed-batch mode. A series of alternate current (AC) electrochemical impedance spectroscopy (EIS) tests, direct current (DC) electrochemical methods such as potentiodynamic polarization, cyclic voltammetry (CV), and linear polarization resistance, and imaging techniques have been used to investigate the underlying mechanisms that enable the 2D hBN coatings to protect metals against harsh MIC conditions. Finally, we demonstrate that the single-layered hBN coatings suppress galvanic corrosion effects that are typically encouraged by single-layered graphene (SLG) coatings.

RESULTS AND DISCUSSION

Characterization of Atomic Layers of Hexagonal Boron Nitride.

The low-magnification image in Figure 1a

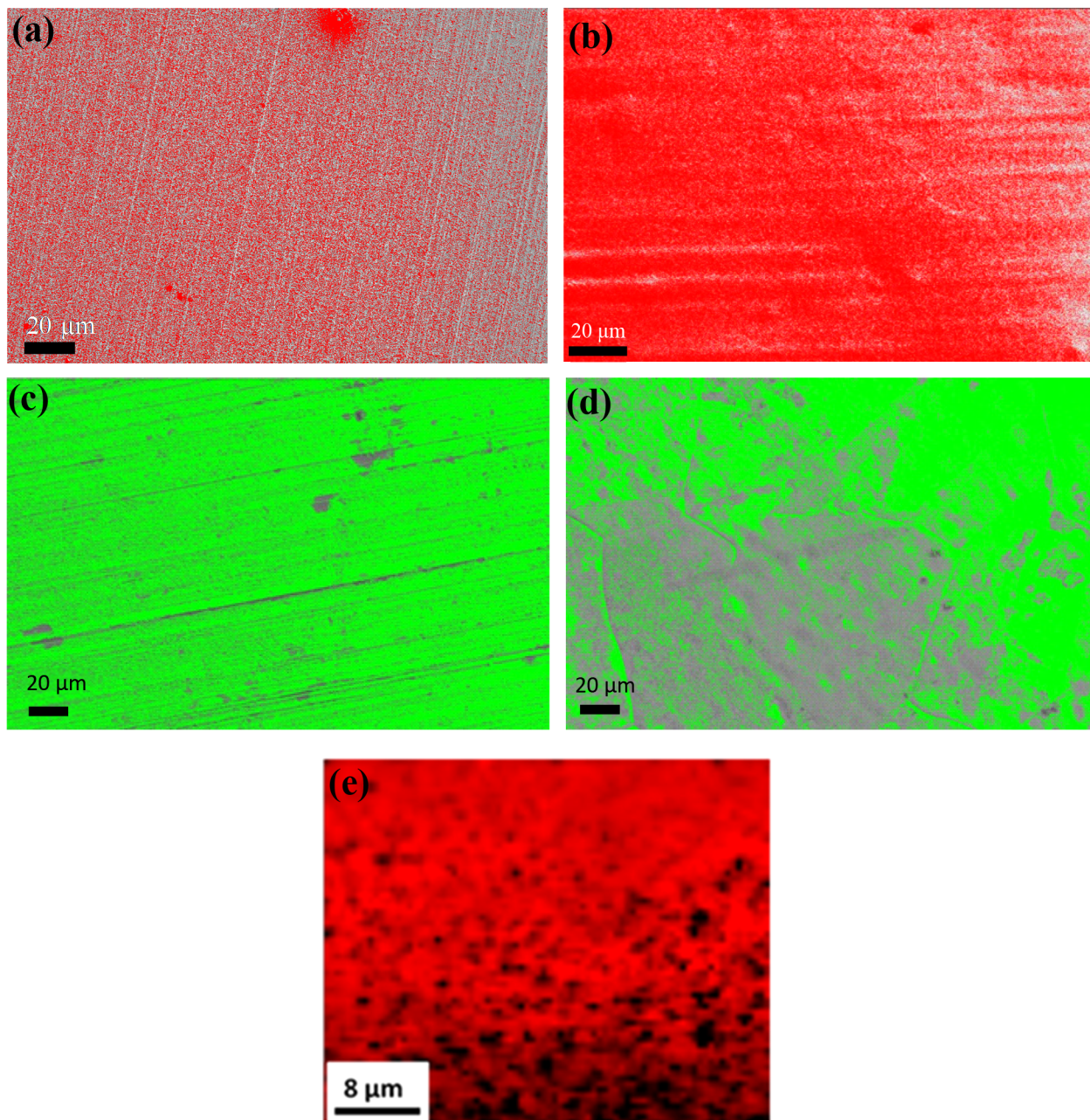


Figure 2. SEM images after air annealing ($200\text{ }^{\circ}\text{C}$, 8 h) for (a) Bare Cu showing 70% of oxidized surface (b) SL-hBN-Cu showing 30% of oxidized surface. Note: White area indicates oxidized copper and red area indicates protected copper. SEM images after 30% H_2O_2 exposure (2 h) for (c) Bare Cu showing 71% of oxidized surface (d) SL-hBN-Cu showing 45% of oxidized surface. Note: Green area indicates oxidized copper and gray area indicates protected copper. (e) Raman spectra of a transferred CVD hBN film on SiO_2/Si showing surface coverage of $\sim 1488\text{ }\mu\text{m}^2$ for hBN (equivalent to $\sim 88\%$ surface coverage). WITEC 300R Confocal Raman Imaging was used with a laser wavelength of 532 nm and 100 \times objective lens.

show a monolayer of conformal hBN coatings deposited over Cu foils by chemical vapor deposition (CVD). The Cu grain boundaries are indicated with yellow arrows and the copper domains as dark patches (Figure 1a,b). The higher-magnification image in Figure 1b shows a monolayer of SL-hBN with large area on the Cu foil. The occasional faint gray zones suggest the presence of bilayers in certain regions. To further confirm the presence of the SL-hBN film on Cu foil, the sample was transferred onto the SiO_2/Si substrate using a poly(methyl methacrylate)-based transfer method. The light indigo shade in Figure 1c indicates a monolayer of hBN, whereas the brown patch indicates the underlying SiO_2/Si substrate through a

topographical defect induced during the transfer. The transmission electron microscopy (TEM) analysis reveals the transparent, aggregated crystalline structure for the hBN coating (Figure 1d). Furthermore, the TEM image shows a folded edge with one line indicating the presence of a layer of hBN (Figure 1e) on the copper foil with a corresponding interlayer spacing of 3.3 Å. These values match the theoretical estimates for distances between lattice planes for bulk hBN.²⁵ The selected area diffraction measurement shown in the TEM image confirm an atomic-scale chicken wire (hexagonal) pattern of hBN on the SL-hBN-Cu (Figure 1f). Finally, the Raman data for the Si/SiO_2 -transferred hBN film analyzed with

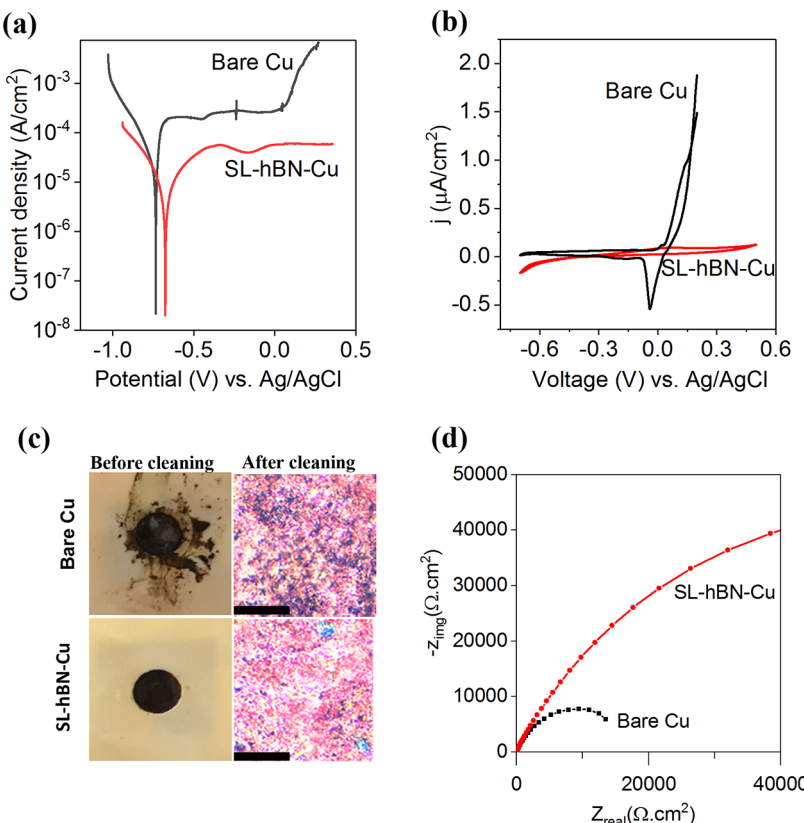


Figure 3. Electrochemical data within 24 h of exposure to sessile SRB-G20 medium. (a) Potentiodynamic polarization and (b) cyclic voltammetry curves for bare Cu and SL-hBN-Cu. (c) Optical images of Bare Cu and SL-hBN-Cu after destructive test. Scale: 20 μm. Potentiodynamic polarization measurements in a potential range of −300 to +1000 mV from open-circuit voltage. Cyclic voltammetry measurements in the potential window of −700 to +200 mV (vs Ag/AgCl) for bare Cu; for SL-hBN, positive potential was extended up to +500 mV. (d) Nyquist plot of Bare-Cu and SL-hBN-Cu.

the Lorentzian peak fitting method¹⁸ confirm the Raman peak at 1370 cm⁻¹ (Figure 1g) that matches a single layer of hBN film.²⁶

Identifying Inherent Defects in SL-hBN. We carried out detailed oxidation experiments to identify the defect density of SL-hBN coatings. The results from the oxidation experiments are summarized here with further details below: (1) SL-hBN coatings were able to protect the underlying copper substrates in oxidizing environments; (2) SL-hBN coatings are characterized by inherent defects; (3) Raman mapping tests corroborate the specific degree of surface coverage offered by the single layer of hBN coating. The oxidation experiments were carried out by exposing the SL-hBN-Cu and bare Cu to oxidizing environments induced by air annealing (~200 °C, ~8 h). Another set of oxidation experiments was carried out by treating the samples with 30% H₂O₂ for ~2 h. The exposure time determined from preliminary trials ensured aggressive oxidizing environments without destroying the samples. Figure 2a,b presents the scanning electron microscopy (SEM) images for the oxidized samples at the end of the air annealing experiments (~200 °C, ~8 h). The oxidized surface is shown as the white layer on the copper substrate (red background). A quantitative analysis using ImageJ software revealed that the percentage of oxidized area for SL-hBN-Cu and bare Cu was ~30 and ~70%, respectively. Exposure to H₂O₂ revealed that SL-hBN-Cu is susceptible to oxidation under aqueous conditions (oxidized surface in green color and unaffected copper in gray color) (Figure 2d). The H₂O₂ experiments revealed that the SL-hBN-Cu and bare Cu were oxidized by

~45 and ~71%, respectively (Figure 2c,d). These results indicate that defects due to grain boundaries and uncoalesced grains (measured in terms of the % copper oxidation) affect the surface coverage offered by the SL-hBN coatings.

We carried out additional Raman mapping tests after transferring the films of SL-hBN-Cu on SiO₂/Si specimens (exposed area ~1431 μm²) (Figure 2e). The Raman mapping results indicate that hBN coatings were characterized with a coverage area of ~88%. Considering this situation, the enhanced performance of the hBN coatings (*i.e.*, lower corrosion rates) is attributable to its insulating nature and its resultant ability to repress galvanic effects (as discussed later). Improving surface coverage is expected to further enhance the ability of hBN coatings to combat MIC.

Crystallographic Orientation of Cu and the Effect on Defects in SL-hBN. The hBN films grown using the CVD process are prone to intercalation of corrosion molecules due to the following two factors: (i) defects that develop due to discontinuous formation of layers in the form of isolated islands or domains and (ii) mismatch of copper and hBN orientation due to polycrystalline copper which introduces different interfaces with hBN, allowing ions to intercalate between the hBN film and copper substrate.^{27–29} Based on previous studies, the lowest defect density for hBN growth on copper requires the Cu surface to have a [111] direction.^{30,31} The single-crystal orientation of Cu helps to match the hexagonal lattice of hBN to produce high-quality and large-scale conformal coating. It eliminates the presence of numerous small-sized grains and grain boundaries which are sources of coating degradation and

increased defect density. The copper foils used for growing hBN have unfavorable crystallographic orientation (Figure S1a,b), which indicates that the as-grown hBN films are also expected to be characterized by defects. To further understand the Cu grain orientations in SL-hBN-Cu, we carried out electron backscattering diffraction mapping (Figure S1b). The mapping for SL-hBN (Figure S1b) was monocrystalline Cu[100]. Future work should involve utilizing CVD substrates with favorable crystallographic orientation in an effort to reduce defects and improve the surface coverage of hBN coatings.

High-Performance, Nanoscale hBN Coatings for Microbially Induced Corrosion Resistance. Sulfate-reducing bacteria represent a diverse group of prokaryotes that are known to accelerate corrosion of technologically relevant metals. We used *D. vibrio* G20 as the model for Gram-negative mesophilic SRB to evaluate the MIC resistance of SL-hBN-coated Cu using the following three experiments: (i) abiotic control; (ii) planktonic cell test (G20 cells in suspension); and (iii) biofilm test (G20 cells encapsulated in a biological film).

Biotic vs Abiotic Corrosion under Neutral Conditions. As discussed in the Supporting Information (Figures S2 and S3), the lactate C media did not exert any corrosive effects on Cu in the absence of the G20 strain (*i.e.*, abiotic conditions). For example, the open-circuit potential (OCP) for the biotic tests shifted to negative values (-750 mV *vs* Ag/AgCl) when compared to that with abiotic tests (0 mV *vs* Ag/AgCl) (Figure S2a). The DC tests show that the polarization resistance (R_p) for biotic tests was ~ 67 times lower compared to its abiotic counterpart (Figure S2b), and corrosion rates (Figure S2c) were ~ 4 times higher. The EIS analysis also suggests that the charge transfer resistance for biotic tests was ~ 6 times lower when compared to that of the abiotic tests (see Bode plots in Figure S3a,b). The EIS analysis for the abiotic and biotic tests indicates different sequences of corrosion mechanisms and different electrical equivalent circuit (EEC) for each case (Figure S3c,d).

Planktonic Tests: Passivation Effects of SL-hBN Coatings. We confirmed the passive nature of SL-hBN coating against the MIC effects of the planktonic cells in five different ways, as discussed below. First, we used potentiodynamic polarization tests to observe the current response of the working electrode after sweeping its applied potential away from the OCP conditions. The nobler OCP value for the SL-hBN-Cu cell (-670 mV *vs* Ag/AgCl) when compared to that of bare copper (-735 mV *vs* Ag/AgCl) supports the passivation property of the SL-hBN coating (Figure 3a). Lower current density in the anodic branch indicates its higher corrosion resistance (Figure 3a). The single-layered hBN coating limits the corrosion current to ~ 6 mA/cm², which is ~ 4 -fold lower compared to that of bare Cu (~ 27 mA/cm²) (Figure 3a). The anodic polarization curve for the bare Cu is dominant at higher applied potentials (starting from 0 V *vs* Ag/AgCl). Moreover, the anodic branch for the bare Cu test registers a sharp increase in current density (at 0 V *vs* Ag/AgCl), indicating the breakdown of the passivation film on the Cu surface and subsequent copper dissolution. In contrast, the current density values for the SL-hBN-Cu remain constant during the entire potential range, confirming its ability to minimize copper dissolution even at higher potential scans.

Second, we ran CV tests for the bare Cu and SL-hBN-Cu cells for four consecutive cycles to investigate the underlying mechanisms for the Cu corrosion. The CV results confirm that the anodic current observed during the potential polarization

tests is due to Cu oxidation ($\text{Cu} \rightarrow \text{Cu}^{2+} + 2e^-$). For example, the CV test for the bare Cu cell yielded a sharp increase in the current density when the potential approached $+30$ mV with an oxidation peak at ~ 144 mV *vs* Ag/AgCl (Figure 3b). This oxidation peak can be attributed to Cu dissolution. The reduction peak (-40 mV *vs* Ag/AgCl) during the negative scan corresponds to the reduction of Cu^{2+} ions. Figure 3b provides the evidence for the ability of the SL-hBN coating to suppress the Cu dissolution. The peak anodic current (i_{pa}) for the SL-hBN coating (~ 25 $\mu\text{A}/\text{cm}^2$) is ~ 36 times lower compared to that of bare Cu (~ 915 $\mu\text{A}/\text{cm}^2$). This anodic peak is absent for the SL-hBN-Cu cell at positive potentials (0 – 500 mV *vs* Ag/AgCl).

Third, we used optical imaging to assess the degree of corrosion attack on the underlying Cu surfaces after four cycles of the CV runs. The CV test represents a destructive electrochemical test. As shown in Figure 3c, the bare Cu suffered a higher degree of debilitation, whereas the SL-hBN-coated Cu stayed intact even after the four CV runs.

Fourth, the post-mortem analysis revealed that the hBN coatings minimized the degree of pitting attack on the underlying Cu surface. We cleaned the surfaces of the corroded specimens (*i.e.*, after the CV runs) with $\sim 10\%$ sulfuric acid to remove remnants of the biofilm and corrosion products. The bare Cu sample was characterized by an extremely rough surface with an abundant number of micropits throughout the sample area, whereas the surface of the SL-hBN sample remained intact, exhibiting only minor surface roughness and isolated pits (Figure 3c).

Finally, EIS analysis was used to discern the protection mechanism offered by SL-hBN coatings against the planktonic cells. As shown in Figure 3d, the magnitude of the Nyquist arc (*i.e.*, polarization resistance (R_p)) in the SL-hBN-Cu cell is 3-fold higher than that of the bare Cu cell. The EEC fitting analysis confirms that the overall corrosion resistance in the SL-hBN-Cu cell ($R_{corr} = \text{charge transfer resistance } (R_{ct}) + \text{pore resistance } (R_{po}) = 52.78 \text{ k}\Omega \cdot \text{cm}^2$) is $\sim 49\%$ higher than that of the bare Cu ($21.13 \text{ k}\Omega \cdot \text{cm}^2$) (Table S1). The impedance spectra in all cases follow a two-time constant model that is connected in series with the solution resistance (R_s) (Figure S3d). The first-time constant describes a pore resistance (R_{po}), which accounts for ionic or electron conductive pathways in copper corrosion products or SL-hBN coating. The constant phase element (Q_{po}) describes the corresponding pore capacitance and represents the ingress of aggressive electrolytes into the porous layers of the coating present on the Cu surface. The second-time constant describes the resistance to charge transfer (R_{ct}) between Cu and the electrolyte and the capacitance due to double-layer phenomenon (C_{dl}).

Biofilm Tests: Microbial Corrosion Resistance of the SL-hBN Coatings. We used the linear polarization resistance method to investigate the effectiveness of the hBN coatings against MIC of the biofilm. At the end of day 24, the R_p offered by the SL-hBN coating ($\sim 20463 \text{ }\Omega \cdot \text{cm}^2$) was ~ 9 times higher than that of bare Cu ($\sim 2373 \text{ }\Omega \cdot \text{cm}^2$) (Figure 4a). Figure 4b shows that the MIC rates in the SL-hBN cell were $\sim 67\%$ lower on day 1, $\sim 82\%$ lower on day 15, and $\sim 87\%$ lower on day 24. The lower corrosion rates suggest the ability to minimize the corrosion attack on the Cu surfaces. The corrosion current (i_{corr}) and corrosion rates were determined using the Stern-Geray equation (eq 1).

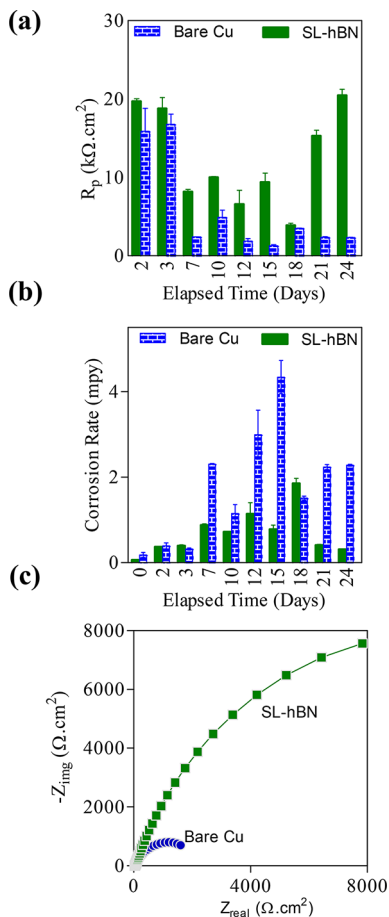


Figure 4. DC and AC corrosion tests establish microbial corrosion resistance of SL-hBN coatings. (a) Polarization resistance data, **(b)** corrosion rates, and **(c)** Nyquist plots for bare Cu and SL-hBN on day 24.

$$i_{corr} = \frac{B}{R_p} \quad (1)$$

The values for the R_p were determined from the slope of the current–potential curve at the open-circuit potential. The value for the constant B was determined using eq 2.

$$B = \frac{\beta_a \beta_c}{2.3(\beta_a + \beta_c)} \quad (2)$$

The Tafel slopes for anodic (β_a) and cathodic branches (β_c) were obtained from the Tafel plot. Finally, the corrosion rates were calculated using eq 3.

$$CR = \frac{K i_{corr}(\text{EW})}{\rho A} \quad (3)$$

where the constant $K = 1.288 \times 10^5$ milli-inches was used to obtain corrosion rates in milli-inches/year (mpy). EW, ρ , and A are the equivalent weight (31.7 g), density (8.94 g/cm³), and area (1 cm²) of the Cu specimen, respectively.

Barrier Properties of hBN Coatings. We used the EIS test as a nonintrusive method for elucidating the reasons for the MIC resistance of the SL-hBN coatings against effects of the G20 biofilm. The hBN coatings exert a dominant electrochemical polarization resistance to underlying corrosion processes relative to the bare Cu cell (Figure 4c). The EEC

analysis confirms that the corrosion resistance (R_{corr}) offered by the hBN coatings ($\sim 27.22 \text{ k}\Omega\cdot\text{cm}^2$) is ~ 10 times higher than that by the bare Cu cell ($\sim 2.53 \text{ k}\Omega\cdot\text{cm}^2$) (Table S2). The value of the Q_{po} for the SL-hBN coating was converted to interfacial capacitance (C_c) using the parallel resistance method developed in an earlier study³² and using the following equation^{32,33}

$$C_c = R_p^{(1-n)/n} Q^{1/n} \quad (4)$$

where C_c is the capacitance of coating film, R_p is the pore resistance, and n is the exponent in the constant phase element.

The following findings imply that the hBN coating offers capacitive impedance behavior and provides a physical barrier to stop aggressive metabolites (e.g., H_2SO_4 and HS^-) from contacting the Cu surface (Table S2).¹³ The value of C_{po} for SL-hBN surface coating is an order of magnitude lower than that of bare Cu. The value of C_{dl} is also ~ 3.4 times lower (Table S2). These findings indicate that the hBN coatings reduce the surface roughness and minimize pathways that relay ions into the underlying Cu surface.³⁴ The χ^2 test confirms an excellent goodness of fit between the measured and predicted values for the EIS data (goodness of fit = 10^{-4} ; average residual <1%) (Figure S4). The compliance of the EIS data with the K–K relations is confirmed by the excellent goodness of fit (10^{-3} using χ^2 value).

We used the R_{corr} value obtained from the EIS analysis to calculate the inhibition efficiency using eq 5. The inhibition efficiency (IE%)¹³ of the single-layered hBN coating was determined to be as high as $\sim 91\%$ (Table S2), which is on par with a commercial coating such as polyaniline used in abiotic environments ($\sim 96\%$).³⁵

$$\text{IE} = \frac{(R_{corr,coated} - R_{corr,bare})}{R_{corr,coated}} \times 100 \quad (5)$$

The optical evidence further corroborates the barrier properties of the hBN coatings against the MIC effects of the biofilm (Figure 5). Both the bare Cu and SL-hBN-Cu surface developed identical biofilm properties related to uniformity and thicknesses (Figure 5a,c). However, the bare Cu surface was characterized by an apparent layer of black corrosion deposits (Figure 5a), whereas the SL-hBN-Cu surface remained clean even after 24 days of the MIC experiment (Figure 5c). Further, the underlying bare Cu surface suffered from localized attack by aggressive SRB metabolites (e.g., organic acids and H_2S), whereas the SL-hBN-Cu specimen faced only a minimal degree of pitting (Figure 5b,d). As discussed below, the X-ray diffraction (XRD) results confirm that the SL-hBN coating remained intact until the end of the MIC experiment. The SL-hBN-coated Cu has also experienced a slight increase in the corrosion rates during the linear polarization resistance tests (Figure 4a,b), which is attributed to the defects in the CVD-coated hBN coatings. Based on the ratio of R_{ct} values for the bare Cu and SL-hBN-Cu,¹² the percentage of the uncoated area on the SL-hBN-Cu surface was estimated to be 9%.

These findings demonstrate that the impermeable nature of the SL-hBN coating prevents the sulfate reducing bacteria and its aggressive metabolic products (acids, HS^-) from contacting the underlying Cu surface. The pore size of the 2D hBN (60 pm)³⁶ is smaller than the effective ionic radii (r) of a range of participating redox species such as Cu^{2+} ($r = 73 \text{ pm}$) and Cu^+ ($r = 77 \text{ pm}$),³⁹ aggressive metabolites such as HS^- ($r = 207 \text{ pm}$),^{37,38} and terminal electron acceptors such as hydronium ion (H_3O^+) ($r = 99 \text{ pm}$).³⁹ As explained in the subsequent

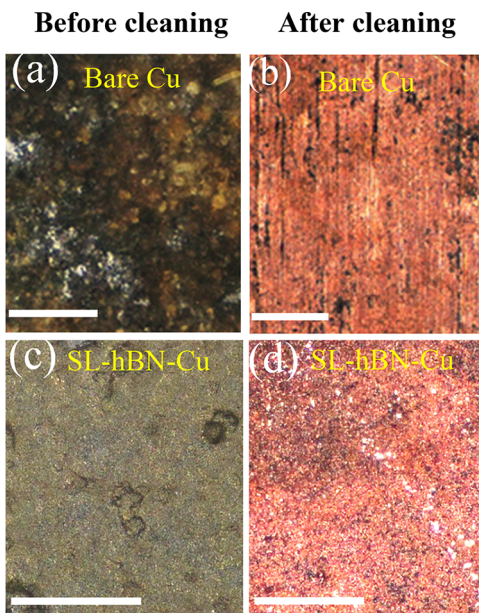


Figure 5. Optical images of bare Cu and SL-hBN-Cu after 12 days of MIC experiment. Corroded bare copper (a) before and (b) after cleaning. MIC-resistant SL-hBN-Cu (c) before and (d) after cleaning. Scale bar: 200 μm .

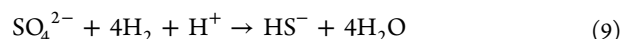
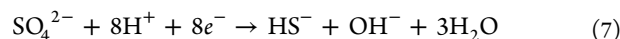
sections of this paper, the MIC resistance of the hBN coating is also attributed to its insulating characteristics that disable the cathodic reactions (*e.g.*, proton reduction) and the subsequent galvanic effects.

Signatures of Microbial Corrosion. At the end of the MIC experiments, the corroded specimens were subjected to visual tests and a series of SEM, energy-dispersive spectroscopy (EDS), and XRD examinations to investigate the signatures of the MIC attack. Both the bare Cu and SL-hBN-Cu electrodes were characterized by thick and homogeneous biofilms of rod-shaped cells that is a typical characteristic of the *D. alaskensis* G20 strain (Figure 6a,b). The visual tests revealed dominant, dark-gray crystals in corrosion deposits representing chalcocite (Cu_2S), which is a signature of the MIC attack on Cu surfaces.^{7,40,41} The EDS analysis of the bare Cu and SL-hBN-Cu surface shows the peaks for sulfur along with other elements including C, Cu, O, and P (Figure 6c,d). We attribute the O and C peaks to the carboxy (C=O and C=O) components of extracellular polymeric (EPS) biofilm.⁷ The X-ray diffractogram of the bare Cu surface confirmed the presence of chalcocite crystals (Figure 6e). The *D. alaskensis* G20 strain also aids in formation of chalcocite and EPS compounds to develop a defensive barrier against Cu toxicity.⁷ The SL-hBN-Cu exhibits a poor signal for the C peak. The intensity of the chalcocite peak for the SL-hBN-Cu surface is also 3 orders of magnitude lower compared to that of the bare Cu (Figure 6f). These results suggest that *D. alaskensis* G20 uses copper as the electron donor (eq 4) and the sulfate or proton as the electron acceptor (eqs 6–8). It participates in a dissimilatory sulfate reduction to generate corrosive hydrogen sulfide (HS^-) species that is responsible for the MIC attack⁴² (eqs 7–9). The lactate is oxidized⁴³ through the lactate dehydrogenase enzyme pathways to produce acetate (eq 11).

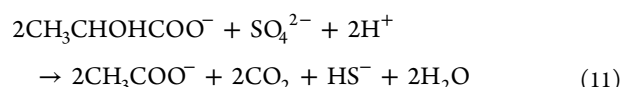
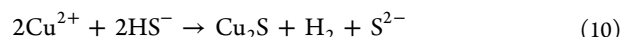
Anodic Oxidation



Cathodic Reduction (in the cytoplasm)



Chalcocite Production



In light of the dissimilatory reduction mechanisms, the following results confirm that the SL-hBN coating decelerates the metabolic activity of SRB, associated production of biogenic sulfide, and subsequent MIC attack by *D. alaskensis* G20. The high-performance liquid chromatography (HPLC) analysis confirms the role of hBN coatings in suppressing the metabolic activities. The electrolyte in the SL-hBN-Cu cell registered ~2-fold lower values for the organic acids (acetic acid and propionic acid) when compared to the bare Cu cell (Figure S5a). The SL-hBN-Cu cell has also registered lower values for sulfide (HS^-) concentration throughout the temporal scale (Figure S5b). For example, the HS^- concentration for the SL-hBN-Cu cell on day 7 (~63 $\mu\text{g/L}$) was ~1.4-fold lower than that of the bare Cu cell (~88 $\mu\text{g/L}$). The rate of increase in the pH for the SL-hBN-Cu cell (7.2 to 7.8) was also lower than that of the bare Cu cell (7.3 to 8.2) (Figure S5c). The lower rate of pH decline indicates the ability of the hBN coatings to retard one or all of the following: (i) conversion of sulfate (a salt of strong acid) to sulfide (a salt of weak base), (ii) conversion of lactic acid ($\text{pK}_a = 3.86$) to acetic acid ($\text{pK}_a = 4.76$), and (iii) proton binding by the sulfides.⁴⁴

Galvanic Corrosion Effects of hBN Coatings Compared with Those of Graphene and Bare Copper. Galvanic corrosion occurs when two dissimilar metals are coupled in a corrosive electrolyte. The metal with more positive potential in a galvanic series will act as a cathode, and the metal with negative potential acts as an anode. Corrosion occurs at the interface of such galvanic couples. A coating such as graphene (graphite) has more noble potential compared to copper in a galvanic series.⁴⁵ A small defect such as pinhole, cracks, or scratches in graphene coating will expose a small anode (Cu) to large cathode (graphene), leading to a large anodic current so as to balance the electron requirement of the cathodic site. The areas with even such minor coating defects are prone to localized corrosion, which will create a ripple effect propagating it to other sites in the metal surface. In fact, recent studies on galvanic effects of graphene described that grain boundary defects in graphene coatings will accelerate localized corrosion by forming galvanic couples.^{45–48}

To study and compare the galvanic effects of graphene and hBN coatings with bare copper, we carried out galvanic corrosion tests using the ASTM G 71-81 standards. These tests were carried out by configuring the Gamry potentiostat in a zero-resistance ammeter mode with transferred single-layer graphene and SL-hBN films on a SiO_2/Si wafer as cathode, bare Cu as anode, and the defined lactate C medium along with the planktonic cells of *Desulfovibrio alaskensis* G20 as the electro-

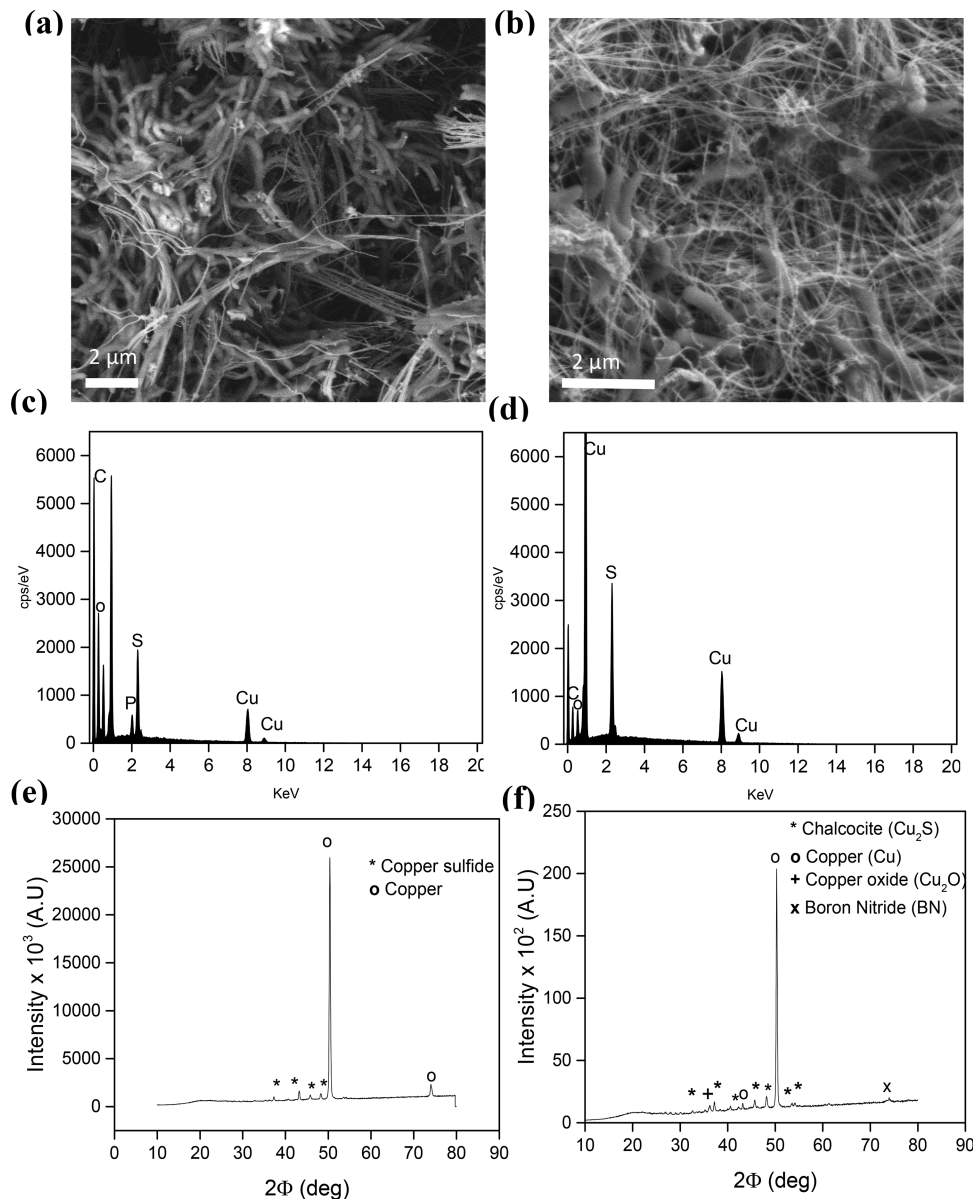


Figure 6. Microbial corrosion signatures. SEM images of G20 biofilm formed on (a) bare Cu and (b) SL-hBN-Cu after 12 days of microbial corrosion experiment. EDS data shows sulfur peaks for (c) bare Cu and (b) SL-hBN. XRD data showing formation of chalcolite compounds on the surfaces of (e) bare Cu and (f) SL-hBN-Cu.

lyte. The procedures for transferring the SLG and SL-hBN films on a SiO_2/Si wafer are depicted in Figure S6. Figure S7 shows the optical images of the transferred SLG and SL-hBN films onto SiO_2/Si wafer. Figure 7 shows a three-electrode galvanic corrosion cell (details in the Methods section) used in this study. SiO_2/Si was used as a control specimen to compare the galvanic current obtained from Cu/SLG and Cu/SL-hBN couples. The galvanic corrosion test was carried out within 24 h of the exposure to *Desulfovibrio alaskensis* G20 lactate C medium with a stable value for the open-circuit potential.

Figure 8a shows that the galvanic current density (I_g) for Cu/SLG ($\sim 32.9 \mu\text{A}/\text{cm}^2$) is ~ 392 times higher compared to that for Cu/SL-hBN ($\sim 8.4 \times 10^{-2} \mu\text{A}/\text{cm}^2$). The higher galvanic current density is directly proportional to higher corrosion rate. The lower galvanic current density in Cu/SL-hBN when compared to that of Cu/SLG clearly demonstrates that hBN coatings are far less vulnerable to galvanic corrosion effects. In fact, the galvanic current and galvanic corrosion rate of the SL-

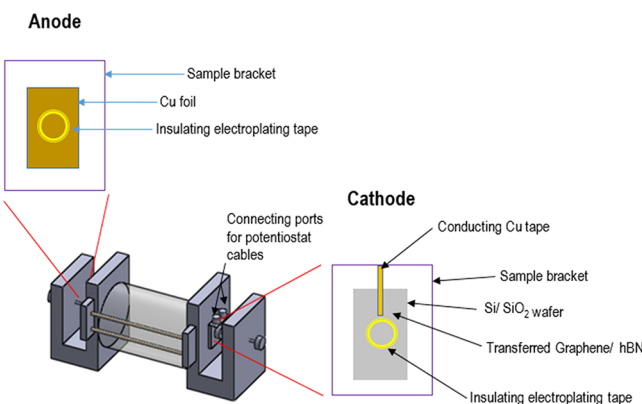


Figure 7. Corrosion cell for galvanic current and potential measurement.

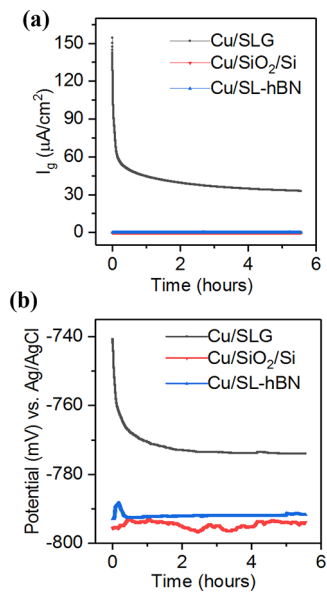


Figure 8. Temporal variation of (a) galvanic current I_g ($\mu\text{A}/\text{cm}^2$) and (b) galvanic potential (mV) for galvanic couples: Cu/SiO₂/Si, Cu/SLG and Cu/SL-hBN in *Desulfovibrio alaskensis* G20 lactate C medium. Cu is used as anode and SiO₂/Si, SLG, and SL-hBN as cathode. The anode to cathode area ratios for all the galvanic couples are maintained at 1.7.

hBN are comparable to those of an insulating SiO₂/Si surface (Table 1), indicating its outstanding insulating characteristics.

Table 1. Galvanic Corrosion Rates Based on Galvanic Couple Current Density

galvanic couple	galvanic current density ($\mu\text{A}/\text{cm}^2$)	galvanic corrosion rate (mpy)
Cu/SiO ₂ /Si	6.22×10^{-3}	2.8×10^{-3}
Cu/SLG	32.9	14.8
Cu/SL-hBN	8.4×10^{-2}	3.79×10^{-2}

The galvanic current density was converted to corrosion rates in mills per year (Table 1) using the Faraday's law as described by procedure ASTM G102.

$$\text{corrosion rate (mpy)} = \frac{K_1 \times I_g \times \text{EW}}{\rho}$$

where K_1 is the Faraday constant (0.1288, mpy), I_g is galvanic corrosion density in $\mu\text{A}/\text{cm}^2$, EW is the equivalent weight of copper (31.7), and ρ is copper density (8.94 g/cm³).

The significantly higher galvanic corrosion rates in the case of Cu/SLG clearly demonstrates that graphene coating on copper leads to galvanic problems. The electrode potential from the galvanic couples' can be used to determine the "higher" cathodic nature of the metal.⁴⁵ The more positive the value of potential in the galvanic couple, the higher its cathodic nature. From Figure 8b, galvanic potential of Cu/SLG is higher (-744 mV) than that of Cu/SL-hBN (-792 mV), which we expect is related to the differences in electrical conductivity of SLG and SL-hBN. Moreover, the galvanic potential of SL-hBN is comparable to that of an insulating SiO₂/Si surface (Figure 8b). Since graphene acts more cathodic when coupled to copper than hBN, Cu/SLG couple generates higher anodic current, leading to greater extent of galvanic corrosion. This is the reason why SL-hBN coatings reduce the galvanic corrosion

effects by ~400 times when compared to SLG coatings, as revealed in our experiments. It should be noted that the electron mobility of hBN ($\sim 4923 \text{ cm}^2/\text{Vs}$)⁴⁹ is ~ 154 -fold lower than that of copper ($\sim 32 \text{ cm}^2/\text{Vs}$)⁵⁰ and ~ 40 times lower than that in graphene ($\sim 2 \times 10^5 \text{ cm}^2/\text{Vs}$).⁵¹ The insulating behavior of hBN is due to the differences in electronegativity between the boron and nitrogen atoms, which results in localization of π -electrons around the nitrogen atoms.⁵²

CONCLUSION

This study demonstrates the ability of single-layered hBN to passivate the negative effects of microbially induced corrosion. It is the thinnest insulating coating that combats the corroding effects of the aggressive metabolites generated by the dissimilatory sulfate reduction process. The MIC resistance of the single-layered hBN coating emerges from the combined effects of its impermeable nature (barrier for electron acceptors, redox species, and biogenic chemicals) and insulating characteristics (suppresses cathodic reduction and galvanic effects).

METHODS

A complete description of the experimental procedures can be found in the Supporting Information, and only a brief account is given below. The copper foils were coated with single-layer hexagonal boron nitride (CVD-2X1-BN; 20 μm thick; Graphene Supermarket) via chemical vapor deposition using the earlier procedures defined in the literature.^{53,54} *D. alaskensis* was anaerobically grown in the lactate C medium using the procedures described previously.^{55,56} Microbial corrosion experiments were carried out in a 400 mL single-compartment corrosion cell consisting of three electrodes: a graphite plate as a counter electrode, a Ag/AgCl as a reference electrode, and a working electrode area of 1 cm^2 . We carried out abiotic tests, planktonic cell tests, and biofilm tests as described in the Supporting Information.

Cyclic voltammetry, linear polarization resistance, potentiodynamic polarization, and electrochemical impedance spectroscopy were used to analyze the resistance of the coatings against MIC conditions. The procedures reported previously⁵⁷ were used to transfer the SL-hBN coatings from an underlying copper foil to the SiO₂/Si substrate. The samples were analyzed using SEM, TEM, XRD, and Raman spectroscopy. To determine the organic, inorganic, anions, and metal ions, we collected the samples of the electrolyte from the test cells periodically using a sterile syringe filter with a pore diameter of 0.2 μm . Concentration of organic acids (lactic, acetic, and propionic acid) was determined using a Shimadzu HPLC equipped with an Aminex HPX-87H column (300 mm \times 7.8 mm dimension), an SPD-10A (UV-vis) detector, and 0.005 M H₂SO₄ as the mobile phase. Concentration of aqueous sulfide was determined using a spectrophotometer following the USEPA methylene blue method.⁵⁸ The pH of the electrolyte samples was measured using an Orion Star Benchtop pH meter.

ASSOCIATED CONTENT

S Supporting Information

The Supporting Information is available free of charge on the ACS Publications website at DOI: 10.1021/acsnano.7b06211.

Detailed methods section, figures (electrochemical tests for bare Cu foil in sterile and *D. alaskensis* media; fitted data for Nyquist plot for bare Cu, SL-hBN; organic acid concentration, sulfide and pH measurements for bare-Cu-cell and SL-hBN-cell; temporal profiles of R_{ct} , pore and double layer capacitance), tables (electrical equivalent circuit parameters for Nyquist plot conducted in planktonic medium for bare Cu and SL-hBN-Cu; EEC

parameters for Nyquist plot conducted in sessile medium for bare Cu and SL-hBN-Cu), and references for the methods section ([PDF](#))

AUTHOR INFORMATION

Corresponding Author

*E-mail: venkata.gadhamshetty@sdsmt.edu.

ORCID

Nikhil A. Koratkar: [0000-0002-4080-3786](#)

Venkataramana Gadhamshetty: [0000-0002-8418-3515](#)

Notes

The authors declare no competing financial interest.

ACKNOWLEDGMENTS

Funding support from National Science Foundation CAREER Award (#1454102), National Aeronautics and Space Administration (NNX16AQ98A), and the South Dakota Board of Regents under the auspices of the Surface Engineering Research Center (SERC) is acknowledged.

REFERENCES

- (1) Krishnamurthy, A.; Gadhamshetty, V.; Mukherjee, R.; Natarajan, B.; Eksik, O.; Shojaei, S. A.; Lucca, D. A.; Ren, W.; Cheng, H.-M.; Koratkar, N. Superiority of Graphene over Polymer Coatings for Prevention of Microbiologically Induced Corrosion. *Sci. Rep.* **2015**, *5*, 13858.
- (2) Heitz, E.; Flemming, H.-C.; Sand, W. *Microbially Influenced Corrosion of Materials: Scientific and Engineering Aspects*; Springer-Verlag: Heidelberg, 1996; p 475.
- (3) Zhang, D.; Qian, H.; Xiao, K.; Zhou, F.; Liu, Z.; Li, X. Corrosion Inhibition of 304 Stainless Steel by *Paecilomyces Variotii* and *Aspergillus Niger* in Aqueous Environment. *Corros. Eng., Sci. Technol.* **2016**, *51*, 285–290.
- (4) Enzien, M.; Wu, M.; Frank, J.; Pope, D. Nonbiocidal Control of Microbiologically Influenced Corrosion Using Organic Film-Forming Inhibitors. *Proceedings of the National Association of Corrosion Engineers*, 4th ed; NACE International, 1996.
- (5) Rajasekar, A. Biodegradation of Petroleum Hydrocarbon and Its Influence on Corrosion with Special Reference to Petroleum Industry. In *Biodegradation and Bioconversion of Hydrocarbons*; Heimann, K., Karthikeyan, O. P., Muthu, S. S., Eds.; Springer Nature: Singapore, 2017; p 311.
- (6) Zuo, R.; Örnek, D.; Syrett, B.; Green, R.; Hsu, C.-H.; Mansfeld, F.; Wood, T. Inhibiting Mild Steel Corrosion from Sulfate-Reducing Bacteria Using Antimicrobial-Producing Biofilms in Three-Mile-Island Process Water. *Appl. Microbiol. Biotechnol.* **2004**, *64*, 275–283.
- (7) Chen, S.; Wang, P.; Zhang, D. Corrosion Behavior of Copper Under Biofilm of Sulfate-Reducing Bacteria. *Corros. Sci.* **2014**, *87*, 407–415.
- (8) Chilkkoor, G.; Upadhyayula, V. K.; Gadhamshetty, V.; Koratkar, N.; Tysklin, M. Sustainability of Renewable Fuel Infrastructure: A Screening LCA Case Study of Anticorrosive Graphene Oxide Epoxy Liners in Steel Tanks for the Storage of Biodiesel and its Blends. *Environ. Sci.: Processes Impacts* **2017**, *19*, 141–153.
- (9) Donoghue, M. O.; Graham, R. G.; Datta, V. W.; Garrett, R. W.; Garrett, J. W. Field Performance versus Laboratory Testing: A Study of Epoxy Tank and Vessel Linings Used in the Canadian Oil Patch. In *Corrosion 2003*; NACE International: San Diego, CA, 2003.
- (10) Heyer, A. Microbiologically Influenced Corrosion in Ship Ballast Tanks. Ph.D. Dissertation, Delft University of Technology, Delft, Netherlands, 2013.
- (11) Tambe, S.; Jagtap, S.; Chaurasiya, A.; Joshi, K. K. Evaluation of Microbial Corrosion of Epoxy Coating by Using Sulphate Reducing Bacteria. *Prog. Org. Coat.* **2016**, *94*, 49–55.
- (12) Prasai, D.; Tuberquia, J. C.; Harl, R. R.; Jennings, G. K.; Bolotin, K. I. Graphene: Corrosion-Inhibiting Coating. *ACS Nano* **2012**, *6*, 1102–1108.
- (13) Huh, J.-H.; Kim, S. H.; Chu, J. H.; Kim, S. Y.; Kim, J. H.; Kwon, S.-Y. Enhancement of Seawater Corrosion Resistance in Copper Using Acetone-Derived Graphene Coating. *Nanoscale* **2014**, *6*, 4379–4386.
- (14) Raman, R. S.; Banerjee, P. C.; Lobo, D. E.; Gullapalli, H.; Sumandasa, M.; Kumar, A.; Choudhary, L.; Tkacz, R.; Ajayan, P. M.; Majumder, M. Protecting Copper from Electrochemical Degradation by Graphene Coating. *Carbon* **2012**, *50*, 4040–4045.
- (15) Krishnamurthy, A.; Gadhamshetty, V.; Mukherjee, R.; Chen, Z.; Ren, W.; Cheng, H.-M.; Koratkar, N. Passivation of Microbial Corrosion Using a Graphene Coating. *Carbon* **2013**, *56*, 45–49.
- (16) Upadhyayula, V. K.; Meyer, D. E.; Gadhamshetty, V.; Koratkar, N. Screening-Level Life Cycle Assessment of Graphene-Poly (ether imide) Coatings Protecting Unalloyed Steel from Severe Atmospheric Corrosion. *ACS Sustainable Chem. Eng.* **2017**, *5*, 2656–2667.
- (17) Dennis, R. V.; Viyannalage, L. T.; Gaikwad, A. V.; Rout, T. K.; Banerjee, S. Graphene Nanocomposite Coatings for Protecting Low-Alloy Steels from Corrosion. *Am. Ceram. Soc. Bull.* **2013**, *92*, 18–24.
- (18) Mahvash, F.; Eissa, S.; Bordjiba, T.; Tavares, A.; Szkopek, T.; Siaj, M. Corrosion Resistance of Monolayer Hexagonal Boron Nitride on Copper. *Sci. Rep.* **2017**, *7*, 42139.
- (19) Parra, C.; Montero-Silva, F.; Henríquez, R.; Flores, M.; Garín, C.; Ramírez, C.; Moreno, M.; Correa, J.; Seeger, M.; Häberle, P. Suppressing Bacterial Interaction with Copper Surfaces through Graphene and Hexagonal-Boron Nitride Coatings. *ACS Appl. Mater. Interfaces* **2015**, *7*, 6430–6437.
- (20) Shen, L.; Zhao, Y.; Wang, Y.; Song, R.; Yao, Q.; Chen, S.; Chai, Y. A Long-Term Corrosion Barrier with an Insulating Boron Nitride Monolayer. *J. Mater. Chem. A* **2016**, *4*, 5044–5050.
- (21) Kim, G.; Kim, M.; Hyun, C.; Hong, S.; Ma, K. Y.; Shin, H. S.; Lim, H. Hexagonal Boron Nitride/Au Substrate for Manipulating Surface Plasmon and Enhancing Capability of Surface-Enhanced Raman Spectroscopy. *ACS Nano* **2016**, *10*, 11156–11162.
- (22) Liu, Z.; Gong, Y.; Zhou, W.; Ma, L.; Yu, J.; Idrobo, J. C.; Jung, J.; MacDonald, A. H.; Vajtai, R.; Lou, J.; et al. Ultrathin High-Temperature Oxidation-Resistant Coatings of Hexagonal Boron Nitride. *Nat. Commun.* **2013**, *4*, 2541.
- (23) Husain, E.; Narayanan, T. N.; Taha-Tijerina, J. J.; Vinod, S.; Vajtai, R.; Ajayan, P. M. Marine Corrosion Protective Coatings of Hexagonal Boron Nitride Thin Films on Stainless Steel. *ACS Appl. Mater. Interfaces* **2013**, *5*, 4129–4135.
- (24) Zhang, J.; Yang, Y.; Lou, J. Investigation of Hexagonal Boron Nitride as an Atomically Thin Corrosion Passivation Coating in Aqueous Solution. *Nanotechnology* **2016**, *27*, 364004.
- (25) Lin, Y.; Williams, T. V.; Connell, J. W. Soluble, Exfoliated Hexagonal Boron Nitride Nanosheets. *J. Phys. Chem. Lett.* **2010**, *1*, 277–283.
- (26) Gorbachev, R. V.; Riaz, I.; Nair, R. R.; Jalil, R.; Britnell, L.; Belle, B. D.; Hill, E. W.; Novoselov, K. S.; Watanabe, K.; Taniguchi, T.; et al. Hunting for Monolayer Boron Nitride: Optical and Raman Signatures. *Small* **2011**, *7*, 465–468.
- (27) Wlasny, I.; Dabrowski, P.; Rogala, M.; Kowalczyk, P.; Pasternak, I.; Strupinski, W.; Baranowski, J.; Klusek, Z. Role of Graphene Defects in Corrosion of Graphene-Coated Cu (111) Surface. *Appl. Phys. Lett.* **2013**, *102*, 111601.
- (28) Wlasny, I.; Dabrowski, P.; Rogala, M.; Pasternak, I.; Strupinski, W.; Baranowski, J.; Klusek, Z. Impact of Electrolyte Intercalation on the Corrosion of Graphene-Coated Copper. *Corros. Sci.* **2015**, *92*, 69–75.
- (29) Chow, P. K.; Singh, E.; Viana, B. C.; Gao, J.; Luo, J.; Li, J.; Lin, Z.; Elías, A. L.; Shi, Y.; Wang, Z.; et al. Wetting of Mono and Few-layered WS₂ and MoS₂ Films Supported on Si/SiO₂ Substrates. *ACS Nano* **2015**, *9*, 3023–3031.
- (30) Hu, B.; Ago, H.; Ito, Y.; Kawahara, K.; Tsuji, M.; Magome, E.; Sumitani, K.; Mizuta, N.; Ikeda, K.-i.; Mizuno, S. Epitaxial Growth of Large-Area Single-Layer Graphene Over Cu (111)/Sapphire by Atmospheric Pressure CVD. *Carbon* **2012**, *50*, 57–65.
- (31) Song, X.; Gao, J.; Gao, T.; Nie, Y.; Sun, J.; Chen, Y.; Jin, C.; Ding, F.; Zhang, Y.; Liu, Z. Wafer-scale CVD Growth of Monolayer Hexagonal Boron Nitride with Large Domain Size by Cu Foil

- Enclosure Approach; <https://arxiv.org/abs/1501.01740> (accessed August 10, 2017).
- (32) Brug, G.; Van Den Eeden, A.; Sluyters-Rehbach, M.; Sluyters, J. The Analysis of Electrode Impedances Complicated by the Presence of a Constant Phase Element. *J. Electroanal. Chem. Interfacial Electrochem.* **1984**, *176*, 275–295.
- (33) Aneja, K. S.; Böhm, H. M.; Khanna, A.; Böhm, S. Functionalised Graphene as a Barrier Against Corrosion. *FlatChem.* **2017**, *1*, 11–19.
- (34) Schmidt, E.; Shi, S.; Ruden, P. P.; Frisbie, C. D. Characterization of the Electric Double Layer Formation Dynamics of a Metal/Ionic Liquid/Metal Structure. *ACS Appl. Mater. Interfaces* **2016**, *8*, 14879–14884.
- (35) Shabani-Nooshabadi, M.; Mollahoseiny, M.; Safari, Y. Electro-polymerized Coatings of Polyaniline on Copper by Using the Galvanostatic Method and their Corrosion Protection Performance in HCl Medium. *Surf. Interface Anal.* **2014**, *46*, 472–479.
- (36) Yan, K.; Lee, H.-W.; Gao, T.; Zheng, G.; Yao, H.; Wang, H.; Lu, Z.; Zhou, Y.; Liang, Z.; Liu, Z.; et al. Ultrathin Two-Dimensional Atomic Crystals as Stable Interfacial Layer for Improvement of Lithium Metal Anode. *Nano Lett.* **2014**, *14*, 6016–6022.
- (37) Dasent, W. E. *Inorganic Energetics: An Introduction*; Cambridge University Press: Cambridge, 1982; p 78.
- (38) Jenkins, H.; Thakur, K. Reappraisal of Thermochemical Radii for Complex Ions. *J. Chem. Educ.* **1979**, *56*, 576.
- (39) Barrett, J. *Inorganic Chemistry in Aqueous Solution*; The Royal Society of Chemistry: Cambridge, 2003; p 35.
- (40) McNeil, M.; Jones, J.; Little, B. Production of Sulfide Minerals by Sulfate-Reducing Bacteria during Microbiologically Influenced Corrosion of Copper. *Corrosion* **1991**, *47*, 674–677.
- (41) Geesey, G. G.; Lewandowski, Z.; Flemming, H.-C. *Biofouling and Biocorrosion in Industrial Water Systems*; CRC Press: Boca Raton, FL, 1994; p 214.
- (42) Keller, K. L.; Rapp-Giles, B. J.; Semkiw, E. S.; Porat, I.; Brown, S. D.; Wall, J. D. New Model for Electron Flow for Sulfate Reduction in *Desulfovibrio Alaskensis* G20. *Appl. Environ. Microbiol.* **2014**, *80*, 855–868.
- (43) Lee, A. K.; Buehler, M. G.; Newman, D. K. Influence of a Dual-Species Biofilm on the Corrosion of Mild Steel. *Corros. Sci.* **2006**, *48*, 165–178.
- (44) Wikieł, A. J.; Datsenko, I.; Vera, M.; Sand, W. Impact of *Desulfovibrio Alaskensis* Biofilms on Corrosion Behaviour of Carbon Steel in Marine Environment. *Bioelectrochemistry* **2014**, *97*, 52–60.
- (45) Cui, C.; Lim, A. T. O.; Huang, J. A Cautionary Note on Graphene Anti-Corrosion Coatings. *Nat. Nanotechnol.* **2017**, *12*, 834.
- (46) Schriver, M.; Regan, W.; Gannett, W. J.; Zaniewski, A. M.; Crommie, M. F.; Zettl, A. Graphene as a Long-Term Metal Oxidation Barrier: Worse than Nothing. *ACS Nano* **2013**, *7*, 5763–5768.
- (47) Zhou, F.; Li, Z.; Shenoy, G. J.; Li, L.; Liu, H. Enhanced Room-Temperature Corrosion of Copper in the Presence of Graphene. *ACS Nano* **2013**, *7*, 6939–6947.
- (48) Datta, D.; Li, J.; Koratkar, N.; Shenoy, V. B. Enhanced Lithiation in Defective Graphene. *Carbon* **2014**, *80*, 305–310.
- (49) Park, H.; Kim, T. K.; Cho, S. W.; Jang, H. S.; Lee, S. I.; Choi, S.-Y. Large-Scale Synthesis of Uniform Hexagonal Boron Nitride Films by Plasma-Enhanced Atomic Layer Deposition. *Sci. Rep.* **2017**, *7*, 40091.
- (50) Fulay, P.; Lee, J.-K. *Electronic, Magnetic, and Optical Materials*; CRC Press: Boca Raton, FL, 2016; p 56.
- (51) Tan, H.; Wang, D.; Guo, Y. Thermal Growth of Graphene: A Review. *Coatings* **2018**, *8*, 40.
- (52) Hod, O. Graphite and hexagonal Boron-Nitride have the Same Interlayer Distance. Why? *J. Chem. Theory Comput.* **2012**, *8*, 1360–1369.
- (53) Kim, K. K.; Hsu, A.; Jia, X.; Kim, S. M.; Shi, Y.; Hofmann, M.; Nezich, D.; Rodriguez-Nieva, J. F.; Dresselhaus, M.; Palacios, T.; et al. Synthesis of Monolayer Hexagonal Boron Nitride on Cu Foil Using Chemical Vapor Deposition. *Nano Lett.* **2012**, *12*, 161–166.
- (54) Li, X.; Cai, W.; An, J.; Kim, S.; Nah, J.; Yang, D.; Piner, R.; Velamakanni, A.; Jung, I.; Tutuc, E.; et al. Large-Area Synthesis of High-Quality and Uniform Graphene Films on Copper Foils. *Science* **2009**, *324*, 1312–1314.
- (55) Sani, R. K.; Geesey, G.; Peyton, B. M. Assessment of Lead Toxicity to *Desulfovibrio desulfuricans* G20: Influence of Components of Lactate C Medium. *Adv. Environ. Res.* **2001**, *5*, 269–276.
- (56) Burlage, R. S.; Atlas, R.; Stahl, D.; Geesey, G.; Sayler, G. *Techniques in Microbial Ecology*; Oxford University Press: New York, 1998; pp 42–43.
- (57) Kim, K. K.; Hsu, A.; Jia, X.; Kim, S. M.; Shi, Y.; Dresselhaus, M.; Palacios, T.; Kong, J. Synthesis and Characterization of Hexagonal Boron Nitride Film as a Dielectric Layer for Graphene Devices. *ACS Nano* **2012**, *6*, 8583–8590.
- (58) Nielsen, A. H.; Vollertsen, J.; Hvittved-Jacobsen, T. Determination of Kinetics and Stoichiometry of Chemical Sulfide Oxidation in Wastewater of Sewer Networks. *Environ. Sci. Technol.* **2003**, *37*, 3853–3858.